




Asteroseismic masses of four evolved planet-hosting stars using SONG and TESS: resolving the retired A-star mass controversy

Sai Prathyusha Malla ¹★, Dennis Stello,^{1,2,3} Daniel Huber,⁴ Benjamin T. Montet,¹ Timothy R. Bedding ^{2,3}, Mads Fredslund Andersen,³ Frank Grundahl,³ Jens Jessen-Hansen,³ Daniel R. Hey,^{2,3} Pere L. Palle,^{5,6} Licai Deng,⁷ Chunguang Zhang,⁷ Xiaodian Chen,⁷ James Lloyd⁸ and Victoria Antoci ^{3,9}

¹*School of Physics, The University of New South Wales, Sydney NSW 2052, Australia*

²*Sydney Institute of Astronomy (SIfA), School of Physics, University of Sydney, NSW 2006, Australia*

³*Stellar Astrophysics Centre, Department of Physics and Astronomy, Aarhus University, Ny Munkegade, DK-8000 Aarhus C, Denmark*

⁴*Institute for Astronomy, University of Hawai‘i, 2680 Woodlawn Drive, Honolulu, HI 96822, USA*

⁵*Instituto de Astrofísica de Canarias, E-38200 La Laguna, Tenerife, Spain*

⁶*Universidad de La Laguna (ULL), Departamento de Astrofísica, E-38206 La Laguna, Tenerife, Spain*

⁷*Key Laboratory of Optical Astronomy, National Astronomical Observatories, Chinese Academy of Sciences, Beijing 100101, People’s Republic of China*

⁸*Department of Astronomy, Cornell University, Ithaca, NY 14850, USA*

⁹*DTU Space, National Space Institute, Technical University of Denmark, Elektrovej 328, DK-2800 Kgs. Lyngby, Denmark*

Accepted 2020 June 10. Received 2020 May 24; in original form 2019 December 18

ABSTRACT

The study of planet occurrence as a function of stellar mass is important for a better understanding of planet formation. Estimating stellar mass, especially in the red giant regime, is difficult. In particular, stellar masses of a sample of evolved planet-hosting stars based on spectroscopy and grid-based modelling have been put to question over the past decade with claims they were overestimated. Although efforts have been made in the past to reconcile this dispute using asteroseismology, results were inconclusive. In an attempt to resolve this controversy, we study four more evolved planet-hosting stars in this paper using asteroseismology, and we revisit previous results to make an informed study of the whole ensemble in a self-consistent way. For the four new stars, we measure their masses by locating their characteristic oscillation frequency, ν_{\max} , from their radial velocity time series observed by SONG. For two stars, we are also able to measure the large frequency separation, $\Delta\nu$, helped by extended SONG single-site and dual-site observations and new *Transiting Exoplanet Survey Satellite* observations. We establish the robustness of the ν_{\max} -only-based results by determining the stellar mass from $\Delta\nu$, and from both $\Delta\nu$ and ν_{\max} . We then compare the seismic masses of the full ensemble of 16 stars with the spectroscopic masses from three different literature sources. We find an offset between the seismic and spectroscopic mass scales that is mass dependent, suggesting that the previously claimed overestimation of spectroscopic masses only affects stars more massive than about $1.6 M_{\odot}$.

Key words: techniques: radial velocities – stars: evolution – stars: fundamental parameters – stars: oscillations.

1 INTRODUCTION

The study of planet occurrence as a function of host star properties, in particular stellar mass, can improve our understanding of planet formation. For this, we need to study potential planet-hosts with a range of stellar masses. However, finding planets around main-sequence stars that are more massive than about $1.4 M_{\odot}$ can be challenging, not only for the transit method due to the larger stellar radius (Borucki et al. 1996), but particularly for the radial velocity technique, because of the increased line broadening induced by the faster rotation of these stars (Johnson et al. 2006). To overcome this, Johnson et al. (2006) set out to target intermediate-mass stars in the subgiant and red giant evolution phases, which are more favourable to planet detection using radial velocity measurements.

These stars, which they dubbed ‘retired A-stars’, were inferred to be the descendants of main-sequence A- or hot F-type stars.

To find which giants are the descendants of main-sequence A- and hot F-type stars require estimates of stellar mass. However, stellar mass is notoriously difficult to obtain for red giants and late subgiants. Stellar mass is typically estimated by interpolating observed stellar properties such as absolute magnitude, spectroscopy-based metallicity ($[Fe/H]$), effective temperature (T_{eff}), and surface gravity ($\log g$) on to stellar model grids (Allende Prieto & Lambert 1999; Pont & Eyer 2004). However, the stellar models of a large range of masses converge in the red giant regime of the HR diagram such that models with different masses and thus, different evolution speeds are within the observed error box. This led Lloyd (2011) to question the inferred masses of the so-called retired A-star sample, suggesting they could be overestimated by up to 50 per cent (based on a selection of evolved planet-hosting stars from the Exoplanet Orbit Database,¹ Wright et al. 2011).

* E-mail: s.malla@student.unsw.edu.au

¹www.exoplanets.org

Later, Johnson, Morton & Wright (2013) applied an apparent magnitude limit on their sample of subgiants and benchmarked them against a Galactic stellar population model to show that there was no overestimation in the spectroscopic masses of these evolved planet-hosting stars. The imposed apparent magnitude limit increased the relative number of massive stars ($M \gtrsim 1.5 M_{\odot}$) observed in their target sample, and hence Johnson et al. (2013) argued that this limit partially counteracts the otherwise lower number of massive stars expected from their faster evolution. However, Lloyd (2013) repeated the calculation in Lloyd (2011), now using apparent magnitude-limited weights for the isochrone integration. From these recalculations, Lloyd (2013) showed that there are fewer massive stars than found in the literature, irrespective of the limit used in the target selection (volume- or magnitude-limit). Meanwhile, Schlaufman & Winn (2013) determined model-independent masses from space velocity dispersions. They found that the velocity dispersions of their subgiant sample were larger than for their main-sequence A0-F5 stars but consistent with their main sequence F5-G5 sample. Hence, they concluded that their evolved planet-hosting stars are less massive than A0-F5 stars, in agreement with Lloyd (2011). Although not dealing with ensembles like the studies above, Pepper et al. (2017) concluded from a comprehensive full system analysis that KELT-11 is indeed a ‘retired A-star’ with a mass significantly greater than $\sim 1.2 M_{\odot}$. Due to the conflicting results obtained, the debate continued about the true masses of these evolved planet-hosting stars.

While classical spectroscopically based mass determinations can be difficult due to the relatively large uncertainties on the spectroscopic parameters like effective temperature, metallicity and surface gravity, recent breakthroughs in asteroseismology have demonstrated that using asteroseismic measurements can provide more precise stellar masses (Huber et al. 2012; Gaulme et al. 2016; Huber et al. 2017; Yu et al. 2018), independent of stellar models (Stello et al. 2008; Kallinger et al. 2010; Chaplin & Miglio 2013; Basu & Chaplin 2017). Thus, asteroseismology is an obvious approach to resolving the dispute over the masses of these evolved planet-hosting stars.

Despite the precision of asteroseismology, the masses of these stars are still contentious. Johnson et al. (2014) made the first attempt to study the only star (HD 185351) in the *Kepler* field that was among the known intermediate-mass evolved planet-hosting stars previously found by radial velocity (hence amenable to asteroseismic investigation). Unfortunately, only one month of *Kepler* data was available, and no definite conclusion could be made because no unique solution could reconcile all (spectroscopic, seismic, and interferometric) measurements at hand. However, a follow-up study (Hj rtinggaard et al. 2017) with a more comprehensive analysis of the asteroseismic data and associated modelling found a unique solution that reconciled all measurements. They concluded that the disputed spectroscopy-based mass was overestimated by about 15 per cent. Stello et al. (2017) also found that the spectroscopic masses of seven of the eight evolved planet-hosting stars they studied with the ground-based Stellar Observations Network Group (SONG) telescope (Andersen et al. 2016) were 15–20 per cent higher than their corresponding seismic masses. White et al. (2018) determined the masses of 5 evolved planet-hosts based on interferometry and also found the spectroscopic masses from the literature to be 15 per cent larger than their values. On the other hand, Campante et al. (2017) and North et al. (2017) found no apparent difference between the spectroscopic and seismic masses in their sample of stars (not all planet-hosting) observed by K2. Similarly, Ghezzi & Johnson (2015) found the difference between the spectroscopic and seismic mass scales insignificant compared to the uncertainty in the stellar masses they obtained.

In this paper, we further investigate the masses of the evolved planet-hosting stars that were previously called into question. For this purpose, we observed four evolved planet-hosting stars for 1–2 weeks in 2018 using the Tenerife node of the SONG telescope. We used the oscillations to estimate the stellar masses following the approach by Stello et al. (2017). In addition, we observed one star, γ Cep, for 2 months in 2014 from the SONG telescope at Tenerife and again in 2017 for about 3 weeks simultaneously from two SONG nodes (Tenerife and Delingha, China). We use the data from these two independent observations to check the robustness of the initial 1–2-week-based SONG data. For one of the stars in our sample, 24 Sex, we verify our findings of the SONG-based seismic masses against the seismic mass obtained from the *Transiting Exoplanet Survey Satellite* (*TESS*; Ricker et al. 2016). Finally, we combine the results from our seismic analysis with those of Stello et al. (2017) and North et al. (2017) to define an ensemble of 16 stars; this allows us to make the most comprehensive seismic-based analysis of the retired A-star mass controversy to date.

2 TARGET SELECTION AND OBSERVATIONS

We selected our targets from the Exoplanet Orbit Database, which had been the basis for the mass controversy. We used the same selection criteria as Stello et al. (2017) in effective temperature and luminosity (L): $3.65 < \log(T_{\text{eff}}/\text{K}) < 3.75$ (i.e. $4467 \text{ K} > T_{\text{eff}} > 5623 \text{ K}$) and $\log(L/L_{\odot}) > 0.75$ ($L > 5.62 L_{\odot}$). The luminosity of each target was derived from a metallicity-dependent bolometric correction equation (equation 18 of Alonso, Arribas & Mart nez-Roger 1999) assuming negligible extinction, given the proximity of the targets (see Stello et al. 2017 for details). From this initial selection, we chose the four brightest stars with $\log g > 3$ that were not already targeted by Stello et al. (2017). Fig. 1 shows our four new targets, along with solar-metallicity stellar evolution tracks from Stello et al. (2013) derived using MESA (Paxton et al. 2013) with dots spaced equally in age.

We used the SONG nodes in Tenerife (Andersen et al. 2014; Grundahl et al. 2017) and Delingha (Deng et al. 2013) for the observations. Observations made at Tenerife used the  chelle spectrograph of the robotic 1-m Hertzprung SONG telescope operated in a fully automated mode (Fredslund Andersen et al. 2019). Observations made at Delingha used a similar spectrograph, but with a slightly shorter spectral range. The operation of the Delingha telescope was not automated, and the observations were carried with an observer present. An iodine cell was used at both nodes for precise wavelength calibration.

The four new stars in our sample were observed for about 10 d from 2018 March to August. In addition, we observed γ Cep (which was observed by Stello et al. 2017 for 13 d) for a period of 75 d from 2014 August to November, and using the SONG telescopes from Tenerife and Delingha simultaneously for 24 d from 2017 October to November. We combined the dual-site data by shifting each series to a common radial velocity zero-point. The observing parameters are listed in Table 1.

The extraction of 1D spectra and the calculation of radial velocities used the same method as Grundahl et al. (2017). The 1D spectra were extracted with a pipeline written in PYTHON, using C++ routines from Ritter, Hyde & Parker (2014) based on the optimal extraction method by Piskunov & Valenti (2002). The radial velocities were then calculated following the approach by Butler et al. (1996) implemented in the *iSONG* software (Antoci et al. 2013; Grundahl et al. 2017). The radial velocity time series were passed through a high-pass filter with a cut-off frequency of $\sim 3 \mu\text{Hz}$ to prevent

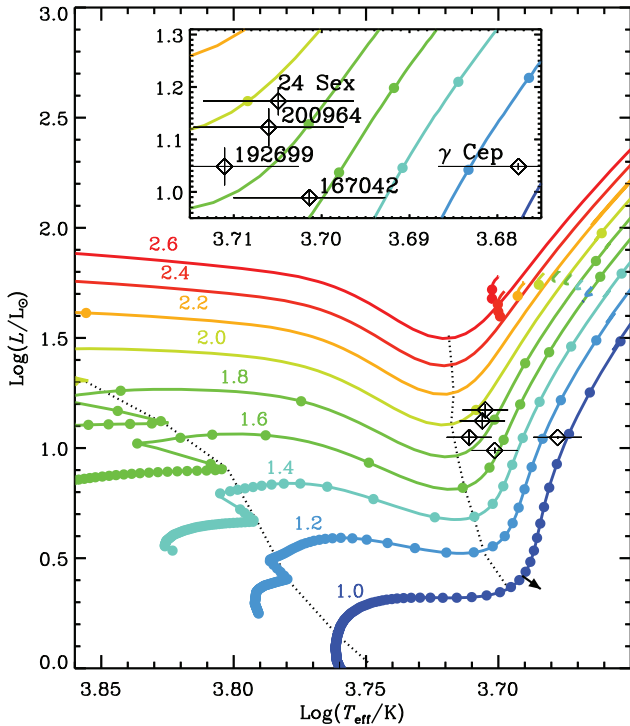


Figure 1. The HR diagram shows the stellar evolution tracks from MESA (Paxton et al. 2013) of solar metallicity from Stello et al. (2013). The filled dots along each track indicate the likelihood of finding a star in a given state of evolution, each separated by 50 million years in stellar age. All masses represented in the figure are in solar units. The track shift when the $[\text{Fe}/\text{H}]$ is increased by 0.2 dex is shown by the black arrow near the bottom of the $1.0 M_{\odot}$ red giant branch. The dotted fiducial lines indicate the transitions from the main sequence to subgiants and from the rapidly cooling subgiants at roughly the same radius to the rapidly expanding red giants at approximately the same T_{eff} . The planet-hosting targets are represented by diamonds, and the black lines indicate the corresponding uncertainties in their luminosities and effective temperatures. The models within the range of luminosities $1.6 \lesssim \log(L/L_{\odot}) \lesssim 1.8$ are the helium-core burning ones. The inset shows a close-up of the targets on the HR diagram.

Table 1. Observing parameters for targets (all Tenerife except where noted).

Star ID	Observation dates	m_v	T_{exp} (s)	N_{exp}	R	$N_{\text{night}}^{\text{obs}}$ (d)	$N_{\text{night}}^{\text{span}}$ (d)	σ_{RV} (m s^{-1})
24 Sex	05/03–17/03/18	6.44	600	404	77k	10	12	6.70
HD 167042	01/06–11/06/18	5.95	900	311	90k	10	10	1.77
HD 192699	27/07–11/08/18	6.45	1200	128	90k	8	16	3.37
HD 200964	17/08–27/08/18	6.49	1200	205	90k	11	11	2.96
γ Cep (2014)	30/08–14/11/14	3.21	180	12647	90k	62	75	2.00
γ Cep	30/10–24/11/17	3.21	180	860	90k	20	23	2.60
γ Cep (Delingha)	30/10–22/11/17	3.21	180	2427	90k	21	24	4.54

Notes. m_v : magnitude

T_{exp} : exposure time

N_{exp} : number of exposures

R : spectrograph resolution

$N_{\text{night}}^{\text{obs}}$: number of observation nights

$N_{\text{night}}^{\text{span}}$: length of time series

σ_{RV} : median radial velocity precision

power leakage in the frequency range of stellar oscillations due to the presence of any slow-moving trends in the data. The final time series after performing a 3σ -clipping are shown in Figs 2 and 3.

The radial velocity variations are typically about $\pm 10 \text{ m s}^{-1}$ and dominated by the oscillations as seen in the inset showing a single-night close-up for HD 192699 (Fig. 2c). The radial velocity time

series for the single-site (2014) data and the dual-site data for γ Cep are shown in Fig. 3.

We also analysed high-precision photometric data from *TESS* for one of our four new stars, 24 Sex. This star was observed in 2-min cadence in Sector 8 from 2019 February 2 to 27. We downloaded the data from MAST² and used the corrected light curve (PDCMAP) for our analysis. The photometric time series was treated in a similar way to the radial velocity time series, the only exception being the application of a high-pass filter with a cut-off frequency of $\sim 50 \mu\text{Hz}$ due to the larger granulation noise levels at lower frequencies for photometric observations. The high-pass filtered time series of the *TESS* data for 24 Sex is illustrated in Fig. 4(a).

3 MEASURING ν_{MAX} AND ITS UNCERTAINTY

Following Stello et al. (2017), we used the same method as Huber et al. (2009) to locate the frequency of maximum oscillation power, ν_{max} . In detail, we calculated the power spectra of the radial velocity time series using a discrete weighted Fourier transform. The resulting power spectra are shown in Figs 4(b), 5, and 6. Using a large frequency separation, $\Delta\nu$, estimated from the approximate $\Delta\nu$ - ν_{max} relation (equation 1 of Stello et al. 2009), we smoothed the power spectrum with a $4\Delta\nu$ wide Gaussian. The highest point of the heavily smoothed power spectrum was taken as ν_{max} (Fig. 5, red dot), and the values are tabulated in Table 2 (column 9).

We tested that the exact choice of the Gaussian smoothing width did not significantly affect our final ν_{max} determination. The test was conducted by varying the Gaussian width by ± 50 percent (corresponding to $2\Delta\nu$), which changed the final ν_{max} estimate by no more than ± 2 percent for three out of the four new stars in our sample. For one star HD 167042, the change was ± 5 percent due to its broader excess power in the oscillation spectrum. We also note that correcting for any power loss due to the averaging effect on oscillations during the integration time, like in the case of *Kepler* long-cadence data (equation 1 of Murphy 2012), only changes the ν_{max} by $\lesssim 1$ percent. Further, Stello et al. (2017) note that their inferred ν_{max} values did not change significantly (less than 1 percent) whether or not one takes the stellar background noise into account (see Stello et al. 2017 for details). This is because the background is very low in radial velocity measurements.

3.1 Estimating ν_{max} uncertainty

Stello et al. (2017) adopted a 15 percent assumed ν_{max} uncertainty based on their investigation of the observations of ξ Hya obtained using the Coralie spectrograph on the Euler Telescope at La Silla (which has a similar performance as SONG; Frandsen et al. 2002). We are now in position to check this assumption using the longer SONG time series for two of the planet-hosting stars reported by Stello et al. (2017): the 75-d long γ Cep data presented in Fig. 3(a), as well as the 110-d long ϵ Tau data from Arentoft et al. (2019). This allows us to divide these long series into shorter segments, each similar in length to those of our main sample of stars (about 10 d). By measuring the scatter in ν_{max} across segments, we can get a realistic estimate of the uncertainty in ν_{max} . This approach is essentially the same as used by Stello et al. (2017) (with the ξ Hya data). However, in our case, the instrumentation and the data reduction approach are identical to that of our shorter observation data sets.

²<https://mast.stsci.edu/portal/Mashup/Clients/Mast/Portal.html>

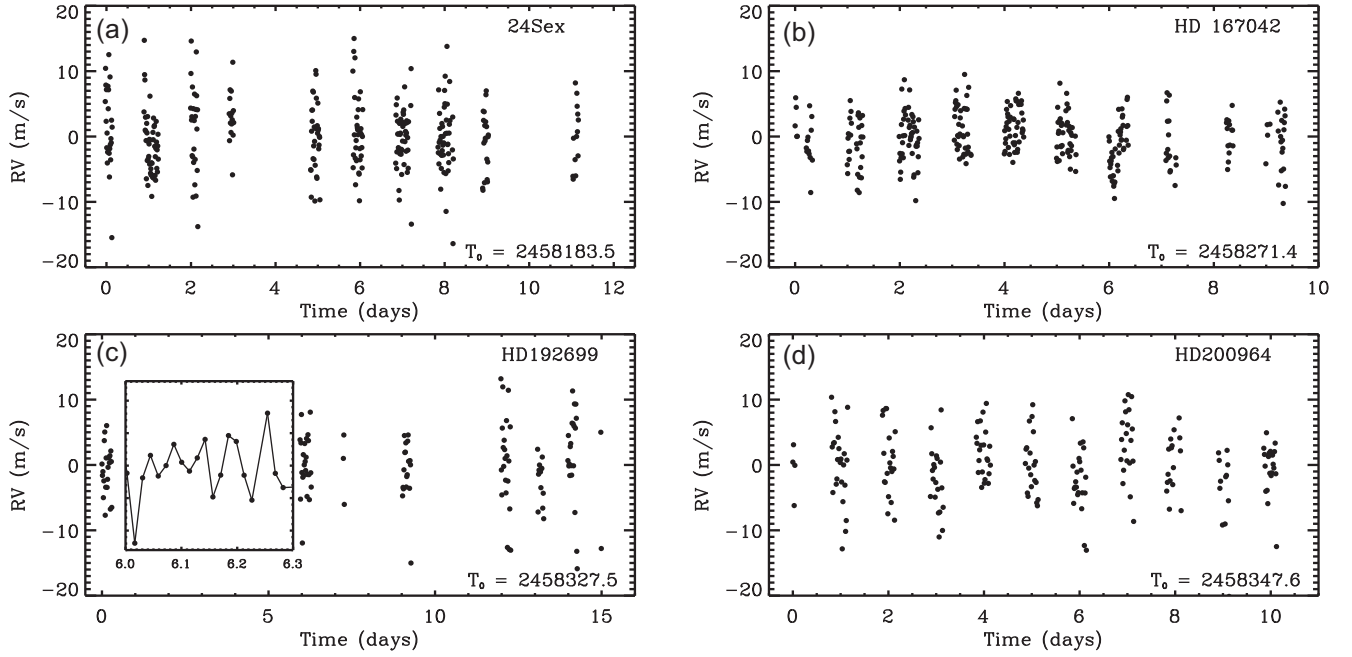


Figure 2. Radial velocity time series for the four new evolved planet-hosting stars studied in this paper. For HD 192699, a single night of observations is shown in the inset. T_0 is the time (BJD) of the first data point. The data can be acquired from the SONG Data Archive (SODA) or from the author upon request.

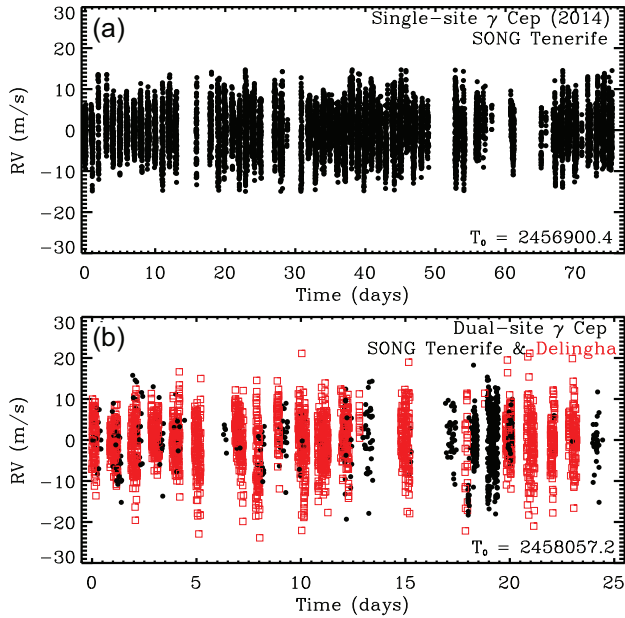


Figure 3. (a) Radial velocity time series for single-site γ Cep, which was observed for a period of 75 d from the SONG node at Tenerife. T_0 is the time (BJD) of the first data point. (b) Combined radial velocity time series for the dual-site γ Cep observations. The filled black circles represent the data from Tenerife, while unfilled red squares represent the data from Delingha. The data can be acquired from the SONG Data Archive (SODA) or from the author upon request.

We split the 75-d long single-site γ Cep time series into segments of 10 d and measure their v_{\max} , treating them as described in Section 3. We observe a v_{\max} scatter of 2.5 per cent across these segments. For the 110-d ϵ Tau data, we found a v_{\max} scatter of 5 per cent also using

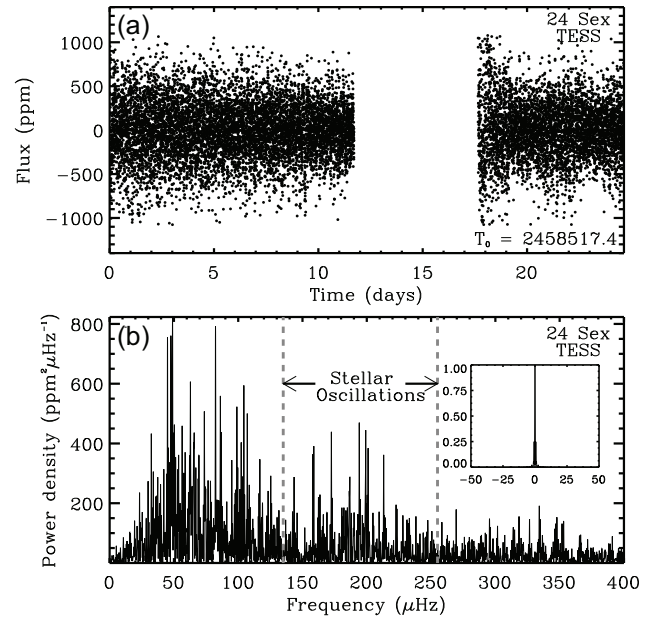


Figure 4. (a) *TESS* light curve of 24 Sex. A high-pass filter of $\sim 50 \mu\text{Hz}$ is applied. T_0 is the time (BJD) of the first data point. The data used here can be obtained from <http://dx.doi.org/10.17909/t9-fnwn-cr91>. (b) Corresponding power density spectrum. The spectral window is in the inset.

10-d segments. Based on the above test on γ Cep and ϵ Tau, we adopt a 5 per cent v_{\max} uncertainty for our four new targets, which is also a typical uncertainty for v_{\max} from photometry (e.g. Huber et al. 2011).

We note that our adopted 5 per cent v_{\max} uncertainty is three times smaller than the 15 per cent v_{\max} uncertainty estimated by Stello et al. (2017) from their analysis of the ξ Hya radial velocity time series.

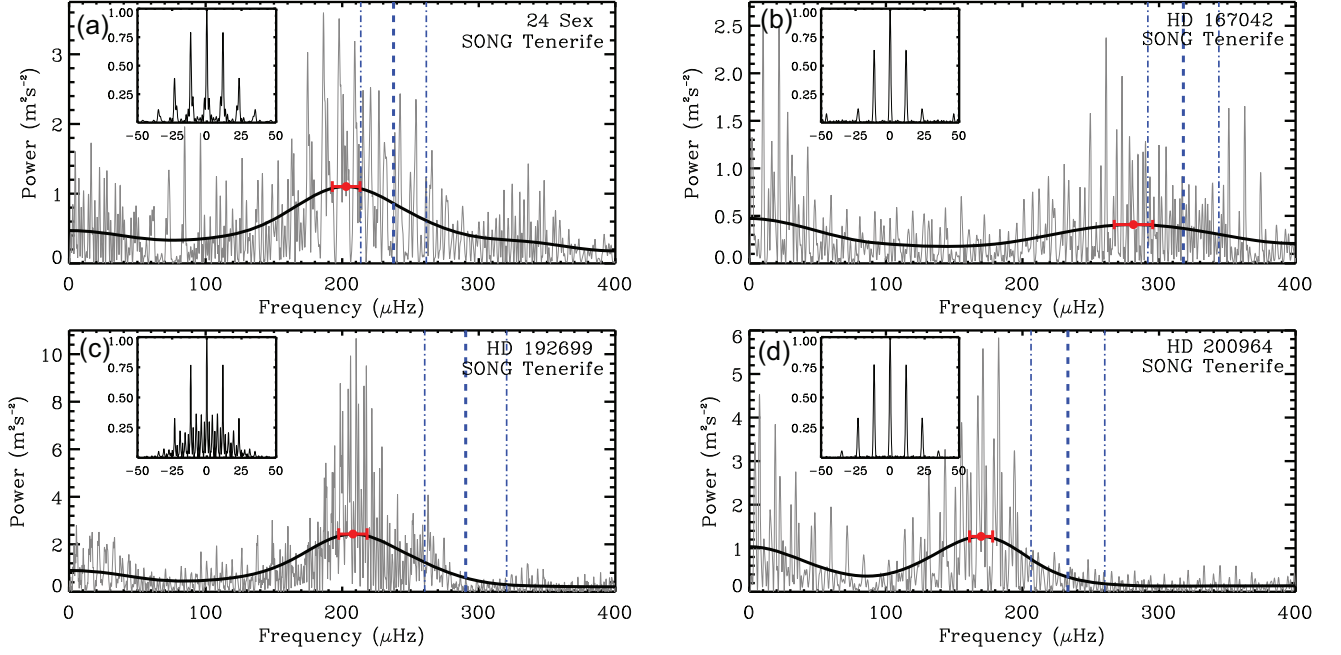


Figure 5. Power spectra of the four new planet-hosting stars observed by SONG. The thick black line is the power spectrum smoothed using a Gaussian of width $4\Delta\nu$. The red dot and the 1σ error bars show the observed ν_{\max} . The thick dashed blue line represents the ν_{\max} predicted from equation (1) using the spectroscopic T_{eff} and mass from the Exoplanet Orbit Database (Table 2, column 8) and the thinner dot-dashed blue lines represent the corresponding uncertainty. The spectral windows are plotted in the insets.

ξ Hya is in a different phase of evolution (secondary clump star) and oscillates at much lower frequencies compared to γ Cep or ϵ Tau. As a result, it has a relatively wide envelope of oscillation power (Yu et al. 2018), and also the data is not densely sampled, leading to a much lower signal-to-noise ratio. These factors may contribute to the larger intrinsic ν_{\max} scatter. In Section 6, we adopt the mass estimates by Stello et al. (2017) for our ensemble analysis, using our newly derived 5 per cent uncertainties. We, therefore, provide an updated summary of the results from Stello et al. (2017) with this fractional uncertainty in Table 3.

4 DERIVING STELLAR MASSES

To calculate stellar seismic mass from the observed ν_{\max} , we used the following scaling relation (Brown et al. 1991; Kjeldsen & Bedding 1995):

$$\frac{\nu_{\max}}{\nu_{\max,\odot}} \simeq \frac{M}{M_{\odot}} \left(\frac{T_{\text{eff}}}{T_{\text{eff},\odot}} \right)^{3.5} \left(\frac{L}{L_{\odot}} \right)^{-1}. \quad (1)$$

Here, we used $\nu_{\max,\odot} = 3090 \mu\text{Hz}$ and $T_{\text{eff},\odot} = 5777\text{K}$ (Huber et al. 2009) to be consistent with Stello et al. (2017). We used *isoclassify*³ (Huber et al. 2017) to compute the luminosity of the stars in our sample using the spectroscopic T_{eff} from the Exoplanet Orbit Database (Table 2, Column 3), *Hipparcos*⁴ parallax (Table 2, Column 5), and *Tycho* V_T photometry as inputs. We set the *dustmap* parameter

³<https://github.com/danxhuber/isoclassify>

⁴For brighter stars ($G < 5$), *Gaia* DR2 parallaxes are known to have larger uncertainties and significant systematic errors due to calibration issues (Drimmel, Bucciarelli & Inno 2019). Four of the stars in our ensemble study in Section 6 have $G < 5$. In addition, β Gem does not have a *Gaia* DR2 parallax measurement. For the rest of the stars, we find the *Hipparcos* parallaxes to be in good agreement with the *Gaia* parallaxes. Therefore, we use *Hipparcos* parallaxes instead of *Gaia*, for consistency.

to ‘allsky’, which enables the use of a combination of reddening maps from Drimmel, Cabrera-Lavers & López-Corrodoira (2003), Marshall et al. (2006), Green et al. (2015), and Bovy et al. (2016) implemented in the *mwdust* package by Bovy et al. (2016). The luminosity⁵ and the seismic mass are tabulated in Table 2 (columns 7 and 10).

We note that the location of the seismic signal predicted from the same scaling relation (equation 1) using the spectroscopic T_{eff} and masses from the Exoplanet Orbit Database is consistently larger than the observed ν_{\max} (Fig. 5, dashed blue line). The predicted ν_{\max} is tabulated in Table 2 (column 8). Likewise, the seismic masses based on ν_{\max} (through equation 1) are lower than their spectroscopic counterparts for all the four new stars in our sample.

5 LARGE FREQUENCY SEPARATIONS OF γ CEP AND 24 SEX

Support for our ν_{\max} -based masses could come from measurements of masses from the frequency separation between overtone modes, $\Delta\nu$, which scales with the square root of the mean stellar density. Hence,

$$\frac{\Delta\nu}{\Delta\nu_{\odot}} \simeq \left(\frac{M}{M_{\odot}} \right)^{0.5} \left(\frac{L}{L_{\odot}} \right)^{-0.75} \left(\frac{T_{\text{eff}}}{T_{\text{eff},\odot}} \right)^3. \quad (2)$$

This provides two different measurements of stellar masses from ν_{\max} and $\Delta\nu$ to check if our results are consistent. We can also combine $\Delta\nu$ (equation 2) with ν_{\max} (equation 1) to give a mass with very little

⁵A brief discussion on the reliability of the *isoclassify*-based luminosities is provided in Section A.

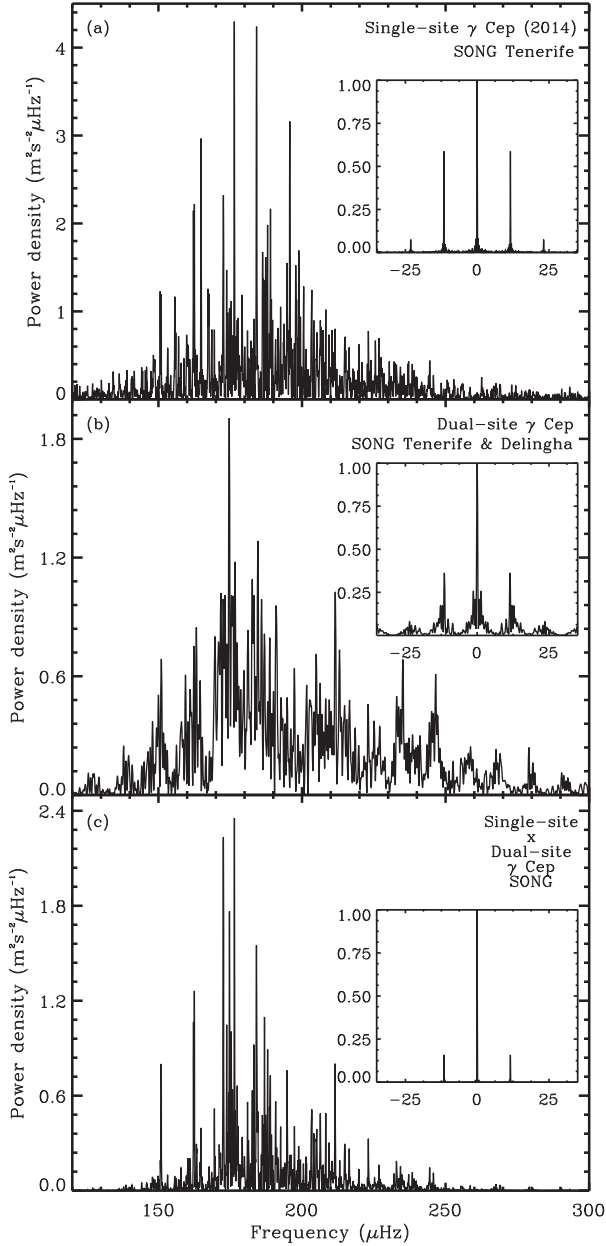


Figure 6. (a) Power density spectrum of single-site γ Cep observations (b) Power density spectrum of dual-site γ Cep data (c) Combined power density spectrum of both γ Cep spectra.

T_{eff} dependence,

$$\frac{M}{M_{\odot}} \simeq \left(\frac{\nu_{\text{max}}}{\nu_{\text{max},\odot}} \right)^3 \left(\frac{\Delta\nu}{\Delta\nu_{\odot}} \right)^{-4} \left(\frac{T_{\text{eff}}}{T_{\text{eff},\odot}} \right)^{1.5}, \quad (3)$$

making the results less sensitive to systematic uncertainties in T_{eff} .

For both equations (2) and (3), it is known that one needs to apply a correction to $\Delta\nu$ in order to obtain a correct mass (Sharma et al. 2016). This comes from the fact that equation (2) is an approximate relation, and stellar models can give a more exact relation for a given star. Here, we use the correction software ASFGRID⁶ by Sharma et al. (2016) to make the appropriate corrections. For the targets selected

using our selection criteria (Section 2), the correction is usually below 2 per cent.

Because the SONG observations of our four new stars are short and single site, $\Delta\nu$ cannot be determined. However, we have long enough time series for γ Cep (both single site and dual site) from SONG and for 24 Sex from *TESS* to measure their $\Delta\nu$.

5.1 γ Cep

Despite the difficulty of measuring $\Delta\nu$ in red giants from ground-based data, our single-site and dual-site data of γ Cep provide an opportunity to do so. For this purpose, we combined those two data sets by multiplying their respective power density spectra, thus retaining the peaks similar in both spectra while reducing the power of those that are not in common. The resulting power density spectra are shown in Fig. 6.

We performed an autocorrelation on the combined power density spectrum to search for regularity. The peak at the frequency shift for which the correlation is the strongest in the vicinity of the $\Delta\nu$ predicted from the $\Delta\nu$ - ν_{max} relation (Stello et al. 2009), is taken as the $\Delta\nu$ peak, and its FWHM gives a conservative uncertainty in $\Delta\nu$. For γ Cep, we obtained a $\Delta\nu$ of $14.28 \pm 0.58 \mu\text{Hz}$, as can be seen from Fig. 7.

Although the autocorrelation allows us to detect $\Delta\nu$, it does so only marginally and does not give any information about where the underlying modes are located in the spectrum. To investigate the regularity in the power density spectrum further, we divided it into segments of length equal to a trial $\Delta\nu$ and stacked them on top of one another. When the trial $\Delta\nu$ corresponded to the correct large frequency separation of the stellar oscillations, modes of the same degree aligned vertically with each other. This diagram, known as an échelle diagram (Grec, Fossat & Pomerantz 1983; Bedding & Kjeldsen 2010), allowed us to clearly see which $\Delta\nu$ provided alignment (a repeated pattern) and showed the absolute location of the aligned peaks. We use the échelle⁷ module (Daniel 2019) to plot the échelle diagrams and test the trial $\Delta\nu$ for which the peaks align vertically. From *Kepler* data, we know there is a correlation between $\Delta\nu$ and the location of the aligned peaks in the échelle diagram (White et al. 2011), which is tighter for red giants (see also Bedding & Kjeldsen 2010; Huber et al. 2010; Mosser et al. 2010) compared to less evolved stars. Hence, the $\Delta\nu$ that we find needs to agree with the correct location of the aligned peaks.

For γ Cep, we tested values of $\Delta\nu$ from 0 to 20 μHz . We found that the peaks stacked neatly on top of one another when $\Delta\nu = 14.25 \mu\text{Hz}$ (Fig. 8a), which is consistent with our results from the autocorrelation. For comparison, we plot the échelle diagram of the *Kepler* star *KIC* 6838375, which has a similar $\Delta\nu$ and ν_{max} as γ Cep (Yu et al. 2018) (Fig. 8b). The long continuous time-base of the *Kepler* data enables us to see the oscillations and identify the modes clearly. We find that the $\Delta\nu$ observed for γ Cep creates an échelle similar to that of the representative star observed by *Kepler* (e.g. aligned peaks at similar locations), except at much lower resolution (due to the shorter time series) and with alias peaks present (due to the non-continuous data of SONG). The latter makes it difficult to determine with certainty which of the peaks in the dipole region are real or aliases. We find one peak that is probably real based on its strength and the location in the échelle (red triangle) as well as

⁶<https://ascl.net/1603.009>

⁷<https://pypi.org/project/echelle/>

Table 2. Observed parameters of the evolved planet-hosting stars.

Star name (1)	log g (dex) (2) ^a	T_{eff} (K) (3) ^a	Literature		M (M_{\odot}) (6) ^a	Derived		Asteroseismology	
			[Fe/H] (dex) (4) ^a	π (mas) (5) ^b		L (L_{\odot}) (7) ^c	$\nu_{\text{max, pre}}$ (μHz) (8)	$\nu_{\text{max, obs}}$ (μHz) (9)	M (M_{\odot}) (10) ^d
24 Sex	3.40 ± 0.13	5069 ± 62	-0.01 ± 0.05	12.91 ± 0.38	1.81 ± 0.08	14.90 ± 0.92	238 ± 24	203 ± 10	1.55 ± 0.16
HD 167042	3.35 ± 0.18	5028 ± 53	0.03 ± 0.04	19.91 ± 0.26	1.63 ± 0.06	9.75 ± 0.27	318 ± 26	281 ± 14	1.44 ± 0.13
HD 192699	3.45 ± 0.07	5141 ± 20	-0.2 ± 0.02	15.24 ± 0.57	1.58 ± 0.04	11.18 ± 0.92	290 ± 30	208 ± 10	1.13 ± 0.13
HD 200964	3.41 ± 0.08	5082 ± 38	-0.2 ± 0.03	13.85 ± 0.52	1.57 ± 0.06	13.28 ± 1.09	233 ± 27	170 ± 8	1.14 ± 0.14

^aSource: Exoplanet Orbit Database, which refers to Mortier et al. (2013). Similar to Stello et al. (2017), we assume $\sigma_{T_{\text{eff}}} = 100$ K and $\sigma_{[\text{Fe}/\text{H}]} = 0.1$ dex to derive columns 7–8 and 10 instead of the quoted uncertainties in T_{eff} and [Fe/H] (Thygesen et al. 2012).

^bSource: *Hipparcos* (van Leeuwen 2007).

^cTo be conservative, we used the largest of the two asymmetric errors obtained from *isoclassify*.

^d ν_{max} -only based asteroseismic masses.

Table 3. Updated Results from Stello et al. (2017).

Star name (1)	ν_{max} (μHz) (2)	M (M_{\odot}) (3)
ϵ Tau	56.9 ± 2.9	2.40 ± 0.22
a Gem	84.5 ± 4.2	1.73 ± 0.17
18 Del	112 ± 6	1.92 ± 0.19
γ Cep	185 ± 9	1.32 ± 0.12
HD 5608	181 ± 9	1.32 ± 0.13
κ CrB	213 ± 11	1.40 ± 0.12
6 Lyn	183 ± 9	1.37 ± 0.14
HD 210702	223 ± 11	1.47 ± 0.14

Table 4. Approximate frequencies of individual modes extracted from the échelle diagrams of γ Cep and 24 Sex.

γ Cep		24 Sex	
Frequency (μHz) (1)	Degree (2)	Frequency (μHz) (3)	Degree (4)
162.5	$l = 0$	158.8	$l = 0$
176.5	$l = 0$	172.5	$l = 0$
190.8	$l = 0$	186.8	$l = 0$
205.1	$l = 0$	201.0	$l = 0$
174.7	$l = 2$	184.3	$l = 2$
189.0	$l = 2$	199.2	$l = 2$
203.4	$l = 2$	213.1	$l = 2$
184.1	$l = 1$	194.1	$l = 1$

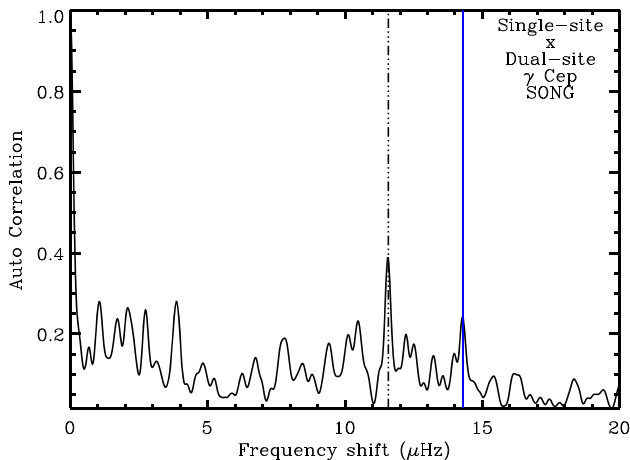


Figure 7. Autocorrelation of the combined power density spectra for γ Cep. The dash-dotted black line represents the daily alias of $11.574 \mu\text{Hz}$ (1 cycle d^{-1}). The solid blue line represents the observed $\Delta\nu$.

the location of the peak that we identify as its alias (white triangle). The approximate frequencies for the individual mode frequencies extracted from the échelle diagram are listed in Table 4.

For γ Cep, we obtain a mass of $1.37 \pm 0.15 M_{\odot}$ when using $\Delta\nu$ alone (from equation 2) and a mass of $1.20 \pm 0.22 M_{\odot}$ when both $\Delta\nu$ and ν_{max} are used (equation 3). These were both in agreement with its previously published ν_{max} -based mass (Stello et al. 2017) even when adopting our new, much smaller ν_{max} uncertainties for the Stello et al. (2017) results (Table 3).

5.2 24 Sex

Compared to ground-based observations, it is relatively easy to measure $\Delta\nu$ in space-based observations due to the availability of continuous data and hence, lower aliases. The 25-d long *TESS* data for one of the stars in our sample, 24 Sex, therefore enables us to measure its $\Delta\nu$.

As for the SONG data of γ Cep, we first calculated the autocorrelation of the power density spectrum of the *TESS* data for 24 Sex. Fig. 9 indicates a strong correlation for a frequency spacing of $14.15 \pm 1.23 \mu\text{Hz}$. We find the best vertical alignment of the modes in the échelle diagram for a $\Delta\nu = 14.10 \mu\text{Hz}$ (Fig. 10).

We obtain a mass of $1.39 \pm 0.23 M_{\odot}$ for 24 Sex based on $\Delta\nu$ (equation 2), and $1.64 \pm 0.38 M_{\odot}$ using both $\Delta\nu$ and ν_{max} . These results are consistent with the ν_{max} -based mass from SONG that we report in Table 2 and hence also lower than the spectroscopic mass.

Overall, we see that the ν_{max} -, $\Delta\nu$ -, and the ' $\Delta\nu + \nu_{\text{max}}$ '-based masses are in good agreement with each other.

6 OFFSET BETWEEN THE SPECTROSCOPIC AND SEISMIC MASSES

From Table 2, we see all four new stars presented here show seismic masses lower than the spectroscopic masses from the Exoplanet Orbit Database. This agrees with the results on seven stars from Stello et al. (2017) but disagrees with the results from North et al. (2017) and the one star in the Stello et al. (2017) sample (γ Cep), for which the seismic and spectroscopic masses agree.

To further investigate these apparently discrepant results, we combine all the results from the previous papers (Stello et al. 2017;

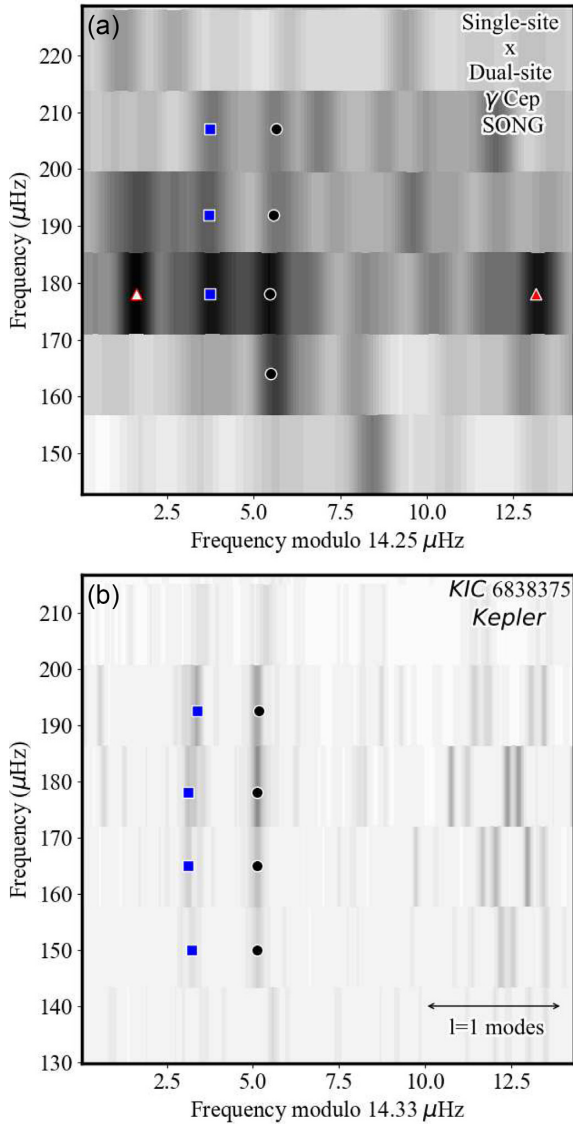


Figure 8. (a) Échelle diagram of γ Cep computed from the combined smoothed power density spectrum. The filled black circles mark the radial ($l = 0$) mode frequencies. The filled blue squares represent the quadrupole ($l = 2$) modes. The filled red triangle represents a dipole ($l = 1$) mode, while the white-filled red triangle represents its alias. Only the modes, which could be clearly distinguished based on their strength and location, are marked. The approximate frequencies corresponding to these modes are provided for reference in Table 4 (columns 1 and 2). (b) Échelle diagram of the *Kepler* star *KIC* 6838375, which has a $\Delta\nu$ similar to γ Cep. Here, we mark the region where the strongest dipole modes fall.

North et al. (2017) with ours, only choosing the stars for which the sources for spectroscopic mass are the same, for consistency.⁸ We show in Figs 11(a) and (b) the mass difference ($M_{\text{seis}} - M_{\text{spec}}$) as a function of the spectroscopic mass (M_{spec}) for the largest sample of stars (16 stars) with a single spectroscopic source that overlap with our combined seismic sample (Mortier et al. 2013). This combined data show an interesting trend. The difference between the two mass scales is insignificant for low-mass stars in agreement with the results

⁸A list of all the stars in the ensemble and their stellar masses across various literature sources used for this study is provided in Table B1.

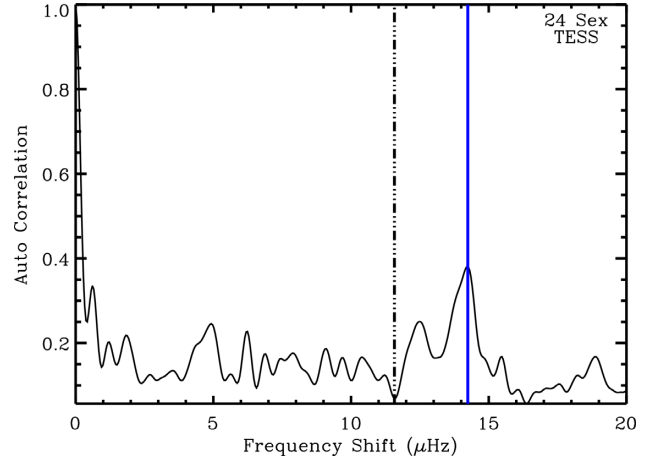


Figure 9. Autocorrelation of the power density spectrum for 24 Sex from *TESS* data. The dash-dotted black line represents the daily aliases of 11.574 μHz (1 cycle d^{-1}), and the solid blue line represents the observed $\Delta\nu$.

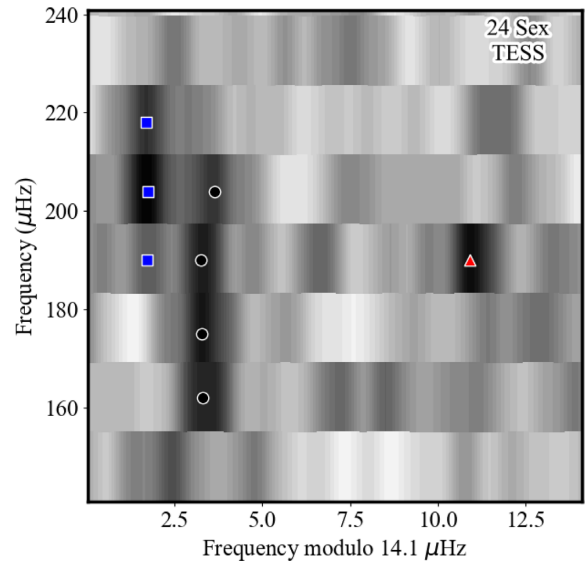


Figure 10. Échelle diagram from the *TESS* data for 24 Sex. The filled black circles mark the radial mode frequencies ($l = 0$), the filled blue squares represent the quadrupole ($l = 2$) modes, and the filled red triangle represents a dipole ($l = 1$) mode. Like for γ Cep, only the modes that could be clearly distinguished based on their strength and location are marked. The approximate frequencies corresponding to these modes are provided in Table 4 (columns 3 and 4).

by North et al. (2017) (and the lowest mass star by Stello et al. 2017). However, for the more massive stars, the difference between the two scales is pronounced, which agrees with the conclusions made by Stello et al. (2017). Here, we note that the majority of stars investigated by North et al. (2017) are of lower mass than those investigated by Stello et al. (2017). We observe a sudden increase in the offset between the two mass scales at about $1.6 M_{\odot}$. Here, we note that Mortier et al. (2013) provided two sets of spectroscopic masses derived using different line lists: one set used the Tsantaki et al. (2013) line list for cooler stars ($T_{\text{eff}} < 5200\text{K}$) and the Sousa et al. (2008) line list for the hotter stars in their sample (Fig. 11a); the other used the Hekker & Meléndez (2007) line list, which was specifically made for giants to avoid blends due to atomic and CN lines (Fig. 11b). The stellar masses from these two different line lists

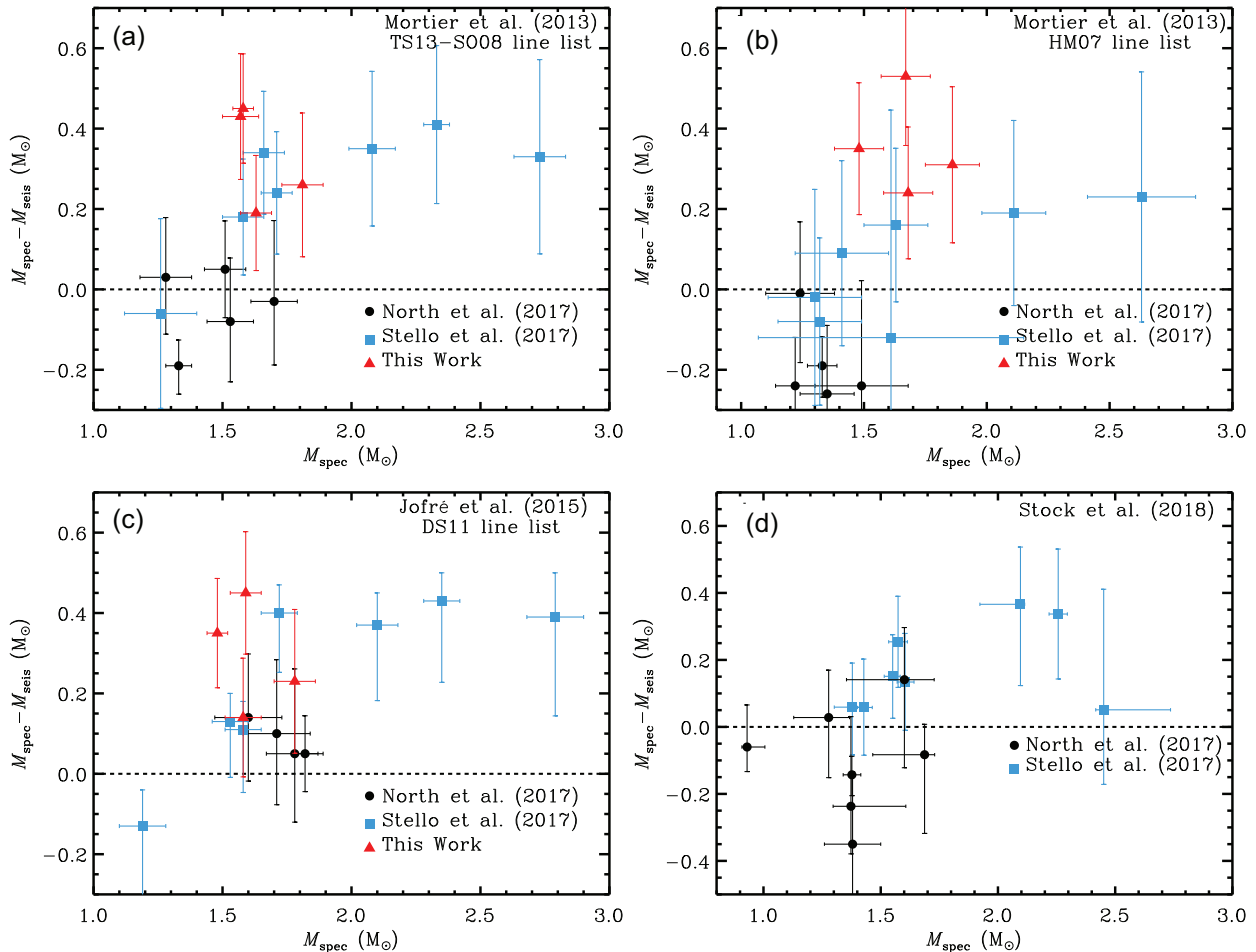


Figure 11. Difference between the spectroscopic and seismic masses plotted as a function of spectroscopic mass from four sources: (a) Mortier et al. (2013), derived using the line lists from Tsantaki et al. (2013, TS13) for cooler stars ($T_{\text{eff}} < 5200$ K), and Sousa et al. (2008, SO08) for hotter stars (16 stars); (b) Mortier et al. (2013), derived using the line list from Hekker & Meléndez (2007, HM07) (16 stars); (c) Jofré et al. (2015), derived using the iron line list from da Silva, Milone & Reddy (2011, DS11) (15 stars); and (d) Stock, Reffert & Quirrenbach (2018), derived using the T_{eff} , $[\text{Fe}/\text{H}]$ and $\log g$ values from Hekker & Meléndez (2007) (15 stars). The results from Stello et al. (2017) with updated error bars and North et al. (2017) have also been included. The filled red triangles represent the results obtained from this paper, the filled black circles represent the results from North et al. (2017), and the filled blue squares denote the results from Stello et al. (2017).

show a slight deviation in the mass range of 1.7–2.1 M_{\odot} (see Fig. 2 of Mortier et al. 2013). By comparing Figs 11(a) and (b) (same method but different line lists), it is evident that the choice of line list matters, but that the mass-dependent offset relative to the seismic mass occurs in both cases. The increasing offset with mass persists even when we adopt other spectroscopic sources, albeit with fewer stars in common with our seismic sample: Jofré et al. (2015) (15 stars, Fig. 11c) and Stock et al. (2018) (15 stars, Fig. 11d). Jofré et al. (2015) derived their spectroscopic masses using the iron line lists from da Silva et al. (2011). Stock et al. (2018) did not use line lists directly in their analysis, but used the T_{eff} , $[\text{Fe}/\text{H}]$, and $\log g$ values from Hekker & Meléndez (2007). Despite a less clear jump at 1.6 M_{\odot} , the comparison with Stock et al. (2018) still shows a slight positive trend with increasing M_{spec} , though barely significant. With a larger sample of 26 stars with seismic data, Stock et al. (2018) found a positive offset with a negative slope, but both the offset and slope were compatible with zero. Hence, they concluded the offset to be insignificant.

Johnson et al. (2010) use the stellar masses from the Spectroscopic Properties of Cool Stars (SPOCS) catalogue (Valenti & Fischer

2005) for their calculation of planet occurrence–mass–metallicity correlation. Of the planet-hosting subgiants studied by Johnson et al. (2010) for their planet occurrence–mass–metallicity correlation, the massive stars ($M \gtrsim 1.6 M_{\odot}$) constitute ~ 46 per cent. Correcting for the observed mass-dependent offset would push the retired A-star sample to smaller masses, which would result in a steeper planet occurrence as a function of stellar mass compared to what was presented by Johnson et al. (2010, equation 8). We found an overlap of 13 stars between our full seismic sample and the spectroscopic sample of Brewer et al. (2016), which is a part of the full SPOCS sample. However, all the stars in the overlap had spectroscopic-based isochrone masses less than 1.7 M_{\odot} and unsurprisingly showing no mass–offset correlation. Hence, no conclusion could be drawn. Further investigation with a larger sample in a range of stellar masses from 1 to 3 M_{\odot} is required to check for the offset between the spectroscopic masses from the SPOCS catalogue and the seismic masses. If an offset exists, a recalculation of the planet occurrence–mass–metallicity correlation will be needed. Such investigation is beyond the scope of the current paper and will be performed in future work (Malla et al. in preparation).

Given that our seismic masses M_{seis} plotted in Fig. 11 are based on ν_{max} , one could suspect that equation (1) provides biased results; either because the different quantities that go into the relation (T_{eff} , L , ν_{max}) are biased or because the relation itself breaks down. However, Stello et al. (2017) previously studied the effect of the potential systematics on ν_{max} . They determined the adopted T_{eff} was unlikely to be off by enough to affect the ν_{max} by such a significant amount as the mass offset we see beyond $1.6 M_{\odot}$ (this is also supported by our consistent masses from equations (1)–(3), given their different dependence on T_{eff}). They noted that a systematic shift in metallicity by 0.1 dex only alters the ν_{max} predicted from spectroscopy by 4 per cent for stars on the red giant branch. They also found it highly unlikely for the ν_{max} scaling relations to be off by 15–20 per cent for red giants. They concluded that the potential systematics only affected the ν_{max} by 4–5 per cent, which is within our adopted uncertainty. Thus, it seems safe to assume the potential systematics in the seismic mass does not cause the observed offset. This has subsequently been supported by the comparison of radii and masses based on equations (1) and (2) with results from *Gaia* (Zinn et al. 2019a) and Galactic stellar populations (Sharma et al. 2019), suggesting even less room for error in equation (1). The sudden jump in stellar rotation speeds, Kraft break, occurs at $1.2 M_{\odot}$ (Kraft 1967), and thus, the observed offset is unlikely to be associated with this jump in rotational velocities either.

The transition mass of $1.6 M_{\odot}$ for the offset is about the same as the one that separates slow- and fast-evolving stars in the lower red giant branch region, which is where most of our ‘retired A-star’ targets lie. From Fig. 1, it is clear that massive stars ($M \gtrsim 1.6 M_{\odot}$) evolved much faster (thus spend less time) in the target region. Given the size of the spectroscopy-based uncertainties and the merging of tracks of different masses on the red giant branch, the typical spectroscopic error box can easily encompass low mass (slow and hence more likely) and high mass (fast and hence less likely) evolving tracks at the same time. Therefore, if the evolution speeds are not properly accounted for, the inferred stellar masses can be easily overestimated (Lloyd 2011). Here, we note that Stock et al. (2018), which showed the smallest mass-offset among our comparisons, is the only spectroscopic source that explicitly mention they take the stellar evolution speed into account when estimating the stellar masses.

7 CONCLUSIONS

We used radial velocity time series from the ground-based SONG telescopes to determine the asteroseismic masses of four evolved planet-hosting stars that have not previously been investigated using asteroseismology. Our observations are too short to enable the measurement of the large frequency separation or individual mode frequencies. With especially long or less interrupted data for γ Cep (a star previously reported by Stello et al. 2017) and 24 Sex (a star from our sample that has also been observed by *TESS*), we were able to establish the robustness of the results that were based on the shorter base-line data by independently estimating the stellar mass from $\Delta\nu$ alone and from $\Delta\nu$ and ν_{max} combined.

We found an offset between the spectroscopic and seismic masses above a transition mass of $1.6 M_{\odot}$. Our results are consistent with North et al. (2017), who found no offset for less massive stars, and with Stello et al. (2017), who found an offset for more massive stars. Our results also agree with the more recent result by Campante et al. (2019), who found a *TESS*-based seismic mass of $1.23 \pm 0.15 M_{\odot}$ against a spectroscopic mass of $2.1 \pm 0.1 M_{\odot}$ for the evolved planet-host HD 203949. These results suggest that the spectroscopy-

based stellar masses of massive stars ($M \gtrsim 1.6 M_{\odot}$) are prone to overestimation, which implies that planet occurrence increases even more steeply with host star mass, compared to previous estimates (Johnson et al. 2010; Ghezzi, Montet & Johnson 2018).

TESS is currently observing many of these evolved planet-hosting stars, which will enable us to measure their ν_{max} , and possibly $\Delta\nu$ and individual mode frequencies. By combining these data with the *Gaia* DR2 parallax measurements, we should be able to get more precise mass estimates for an even larger sample of previously reported evolved planet-hosts that bracket the mass around the transition mass to further confirm our finding and recalculate the planet occurrence–mass–metallicity correlation towards intermediate-mass stars.

ACKNOWLEDGEMENTS

This research is based on observations made with the SONG telescopes operated on the Spanish Observatorio del Teide (Tenerife) and at the Chinese Delingha Observatory (Qinghai) by the Aarhus and Copenhagen Universities, by the Instituto de Astrofísica de Canarias, and by the National Astronomical Observatories of China. Funding for the Stellar Astrophysics Centre is provided by The Danish National Research Foundation (Grant agreement no. DNRF106). DS acknowledges support from Australian Research Council. DH acknowledges support by the National Science Foundation (AST-1717000). This research had made use of the Exoplanet Database and the Exoplanet Data Explorer at exoplanets.org. This research also uses data collected by the *TESS* mission, which is funded by NASA Explorer programme and obtained from the Mikulski Archive for Space Telescopes (MAST). STScI is operated by the Association of Universities for Research in Astronomy, Inc., under NASA contract NAS5-26555. Support for MAST for non-*HST* data is provided by the NASA Office of Space Science via grant no. NNX13AC07G and by other grants and contracts. In addition, this research has made use of NASA’s Astrophysics Data System Bibliographic Services.

DATA AVAILABILITY

The SONG data used in this article can be acquired from the SONG Data Archive (SODA) or from the author upon request. The *TESS* data for 24 Sex used in this article can be obtained from <http://dx.doi.org/10.17909/t9-fnwn-cr91>. All the tables in this paper are available on CDS in a machine-readable format.

REFERENCES

- Allende Prieto C., Lambert D. L., 1999, *A&A*, 352, 555
 Alonso A., Arribas S., Martínez-Roger C., 1999, *A&AS*, 140, 261
 Andersen M. F. et al., 2014, *Revista Mexicana de Astronomía y Astrofísica Conference Series, Revista Mexicana de Astronomía y Astrofísica, Instituto de Astronomía, UNAM*. p. 83, preprint ([arXiv:1901.08300](https://arxiv.org/abs/1901.08300))
 Andersen M. F., Grundahl F., Beck A. H., Pallé P., 2016, *Revista Mexicana de Astronomía y Astrofísica Conference Series, Revista Mexicana de Astronomía y Astrofísica, Instituto de Astronomía, UNAM*. p. 54, preprint ([arXiv:1901.08293](https://arxiv.org/abs/1901.08293))
 Antoci V. et al., 2013, *MNRAS*, 435, 1563
 Arentoft T. et al., 2019, *A&A*, 622, A190
 Basu S., Chaplin W. J., 2017, *Asteroseismic Data Analysis: Foundations and Techniques*, Princeton University Press
 Bedding T. R., Kjeldsen H., 2010, *Commun. Asteroseismol.*, 161, 3
 Borucki W. J., Dunham E. W., Koch D. G., Cochran W. D., Rose J. D., Cullers D. K., Granados A., Jenkins J. M., 1996, *Ap&SS*, 241, 111
 Bovy J., Rix H.-W., Green G. M., Schlafly E. F., Finkbeiner D. P., 2016, *ApJ*, 818, 130

- Brewer J. M., Fischer D. A., Valenti J. A., Piskunov N., 2016, *ApJS*, 225, 32
- Brown T. M., Gilliland R. L., Noyes R. W., Ramsey L. W., 1991, *ApJ*, 368, 599
- Butler R. P., Marcy G. W., Williams E., McCarthy C., Dosanji P., Vogt S. S., 1996, *PASP*, 108, 500
- Campante T. L. et al., 2017, *MNRAS*, 469, 1360
- Campante T. L. et al., 2019, *ApJ*, 885, 31
- Casagrande L., VandenBerg D. A., 2018, *MNRAS*, 475, 5023
- Chaplin W. J., Miglio A., 2013, *ARA&A*, 51, 353
- da Silva R., Milone A. C., Reddy B. E., 2011, *A&A*, 526, A71
- Daniel R. Hey, 2019, Zenodo, d anhey/echelle: Initial release
- Deng L. et al., 2013, in Burton M. G., Cui X., Tothill N. F. H., eds, Proc. IAU Symp. 288, Astrophysics from Antarctica, Cambridge University Press, p. 318
- Drimmel R., Cabrera-Lavers A., López-Corrodoira M., 2003, *A&A*, 409, 205
- Drimmel R., Bucciarelli B., Inno L., 2019, *Res. Notes Am. Astron. Soc.*, 3, 79
- Frandsen S. et al., 2002, *A&A*, 394, L5
- Fredslund Andersen M., Handberg R., Weiss E., Frandsen S., Simón-Díaz S., Grundahl F., Pallé P., 2019, *PASP*, 131, 045003
- Gaulme P. et al., 2016, *ApJ*, 832, 121
- Ghezzi L., Johnson J. A., 2015, *ApJ*, 812, 96
- Ghezzi L., Montet B. T., Johnson J. A., 2018, *ApJ*, 860, 109
- González Hernández J. I., Bonifacio P., 2009, *A&A*, 497, 497
- Grec G., Fossat E., Pomerantz M. A., 1983, *Sol. Phys.*, 82, 55
- Green G. M. et al., 2015, *ApJ*, 810, 25
- Grundahl F. et al., 2017, *ApJ*, 836, 142
- Hekker S., Meléndez J., 2007, *A&A*, 475, 1003
- Hjørringgaard J. G., Silva Aguirre V., White T. R., Huber D., Pope B. J. S., Casagrande L., Justesen A. B., Christensen-Dalsgaard J., 2017, *MNRAS*, 464, 3713
- Huber D. et al., 2010, *ApJ*, 723, 1607
- Huber D. et al., 2011, *ApJ*, 731, 94
- Huber D. et al., 2012, *ApJ*, 760, 32
- Huber D. et al., 2017, *ApJ*, 844, 102
- Huber D., Stello D., Bedding T. R., Chaplin W. J., Arentoft T., Quirion P. O., Kjeldsen H., 2009, *Commun. Asteroseismol.*, 160, 74
- Jofré E., Petrucci R., Saffe C., Saker L., Artur de la Villarmois E., Chavero C., Gómez M., Mauas P. J. D., 2015, *A&A*, 574, A50
- Johnson J. A. et al., 2014, *ApJ*, 794, 15
- Johnson J. A., Marcy G. W., Fischer D. A., Henry G. W., Wright J. T., Isaacson H., McCarthy C., 2006, *ApJ*, 652, 1724
- Johnson J. A., Aller K. M., Howard A. W., Crepp J. R., 2010, *PASP*, 122, 905
- Johnson J. A., Morton T. D., Wright J. T., 2013, *ApJ*, 763, 53
- Kallinger T. et al., 2010, *A&A*, 509, A77
- Kjeldsen H., Bedding T. R., 1995, *A&A*, 293, 87
- Kraft R. P., 1967, *ApJ*, 150, 551
- Lloyd J. P., 2011, *ApJ*, 739, L49
- Lloyd J. P., 2013, *ApJ*, 774, L2
- Marshall D. J., Robin A. C., Reylé C., Schultheis M., Picaud S., 2006, *A&A*, 453, 635
- Mortier A., Santos N. C., Sousa S. G., Adibekyan V. Z., Delgado Mena E., Tsantaki M., Israelian G., Mayor M., 2013, *A&A*, 557, A70
- Mosser B. et al., 2010, *A&A*, 517, A22
- Murphy S. J., 2012, *MNRAS*, 422, 665
- North T. S. H. et al., 2017, *MNRAS*, 472, 1866
- Paxton B. et al., 2013, *ApJS*, 208, 4
- Pepper J. et al., 2017, *AJ*, 153, 215
- Piskunov N. E., Valenti J. A., 2002, *A&A*, 385, 1095
- Pont F., Eyer L., 2004, *MNRAS*, 351, 487
- Ricker G. R. et al., 2016, *Space Telescopes and Instrumentation 2016: Optical, Infrared, and Millimeter Wave*, SPIE, Bellingham, p. 99042B
- Ritter A., Hyde E. A., Parker Q. A., 2014, *PASP*, 126, 170
- Schlaufman K. C., Winn J. N., 2013, *ApJ*, 772, 143
- Sharma S. et al., 2019, *MNRAS*, 490, 2471
- Sharma S., Stello D., Bland-Hawthorn J., Huber D., Bedding T. R., 2016, *ApJ*, 822, 15
- Sousa S. G. et al., 2008, *A&A*, 487, 373
- Stello D. et al., 2013, *ApJ*, 765, L41
- Stello D. et al., 2017, *MNRAS*, 472, 4110
- Stello D., Bruntt H., Preston H., Buzasi D., 2008, *ApJ*, 674, L53
- Stello D., Chaplin W. J., Basu S., Elsworth Y., Bedding T. R., 2009, *MNRAS*, 400, L80
- Stock S., Reffert S., Quirrenbach A., 2018, *A&A*, 616, A33
- Thygesen A. O. et al., 2012, *A&A*, 543, A160
- Tsantaki M., Sousa S. G., Adibekyan V. Z., Santos N. C., Mortier A., Israelian G., 2013, *A&A*, 555, A150
- Valenti J. A., Fischer D. A., 2005, *ApJS*, 159, 141
- van Leeuwen F., 2007, *Hipparcos, the New Reduction of the Raw Data*. Vol. 350, Springer, Netherlands
- White T. R. et al., 2018, *MNRAS*, 477, 4403
- White T. R., Bedding T. R., Stello D., Christensen-Dalsgaard J., Huber D., Kjeldsen H., 2011, *ApJ*, 743, 161
- Wright J. T. et al., 2011, *PASP*, 123, 412
- Yu J., Huber D., Bedding T. R., Stello D., Hon M., Murphy S. J., Khanna S., 2018, *ApJS*, 236, 42
- Zinn J. C., Pinsonneault M. H., Huber D., Stello D., 2019a, *ApJ*, 878, 136
- Zinn J. C., Pinsonneault M. H., Huber D., Stello D., Stassun K., Serenelli A., 2019b, *ApJ*, 885, 166

APPENDIX A: A NOTE ON THE RELIABILITY OF ISOCCLASSIFY-BASED LUMINOSITIES

To test the reliability of the luminosities obtained using *isoclassify*, we ran the analysis again using *Tycho* B_T photometry instead of *Tycho* V_T . Fig. A1(a) shows the fractional difference in the luminosity thus obtained using *isoclassify* based on B_T ($L_{B_T, \text{isoclassify}}$) and on V_T photometry ($L_{V_T, \text{isoclassify}}$), as a function of the latter. We note an average difference of 3.4 per cent between the two, which is less than our adopted uncertainty of 5 per cent.

isoclassify uses the MIST grids⁹ to interpolate bolometric corrections from spectroscopic T_{eff} , surface gravity $\log g$, metallicity $[\text{Fe}/\text{H}]$, and extinction A_V . Zinn et al. (2019b) found the MIST K_s -band bolometric fluxes derived using the corresponding bolometric corrections to be consistent with the bolometric corrections from the InfraRed Flux Method, g -band MIST and another K_s -band bolometric corrections from González Hernández & Bonifacio (2009) within 4 per cent (see Fig. 14 of Zinn et al. 2019b). They also showed that MIST bolometric corrections are consistent with each other within 3 per cent (for i , g , and r bands). Therefore, it would seem safe to assume the *Tycho* V_T and B_T bolometric corrections from the MIST grids to be consistent with other sources of bolometric corrections.

As an additional test, we checked how different bolometric corrections for V_T affect the derived luminosities for our test sample of 12 stars. For these 12 stars, we obtained bolometric corrections from the Casagrande & VandenBerg (2018) tables covering *Tycho* V_T passbands. We then used these bolometric corrections to compute the luminosities (L_{CV18}). Fig. A1(b) demonstrates the fractional difference in L_{CV18} and $L_{V_T, \text{isoclassify}}$ as a function of the latter. We note that the average fractional difference between these two luminosities is 1.3 per cent, which is below our adopted uncertainty.

⁹http://waps.cfa.harvard.edu/MIST/model_grids.html

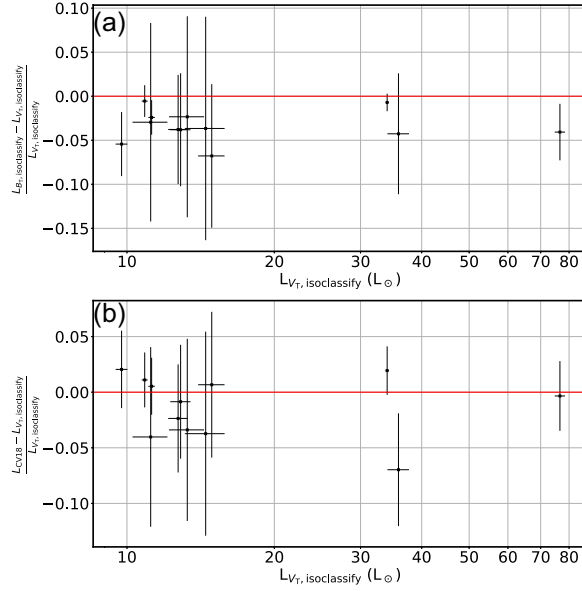


Figure A1. (a) Fractional difference in luminosities derived from *isoclassify* using *Tycho* B_T and V_T photometry as a function of the V_T -based luminosity. The solid red line represents zero difference. (b) Fractional difference in the luminosities derived using Casagrande & Vandenberg (2018) bolometric corrections in the *Tycho* V_T passbands using the MARCS models and the luminosity derived from *isoclassify* for the *Tycho* V_T as a function of the latter.

APPENDIX B: STELLAR MASSES FOR THE ENSEMBLE OF EVOLVED PLANET-HOSTING STARS ACROSS DIFFERENT SOURCES IN LITERATURE

Table B1. Stellar masses for the evolved planet-hosting stars used for the ensemble study in Section 6 across various literature sources.

Star name	Spectroscopy-based grid-based modelling			Asteroseismology	
	Mortier et al. (2013) TS13-SO08 (M_\odot) (2) ^a	Mortier et al. (2013) HM07 (M_\odot) (3) ^b	Jofré et al. (2015) DS11 (M_\odot) (4) ^c	Stock et al. (2018) (M_\odot) (5) ^d	(M_\odot) (6)
24 Sex	1.81 ± 0.08	1.86 ± 0.11	1.78 ± 0.08	–	1.55 ± 0.16^e
HD 167042	1.63 ± 0.06	1.68 ± 0.10	1.58 ± 0.07	–	1.44 ± 0.13^e
HD 192699	1.58 ± 0.04	1.48 ± 0.10	1.48 ± 0.04	–	1.13 ± 0.13^e
HD 200964	1.57 ± 0.07	1.67 ± 0.10	1.59 ± 0.06	–	1.14 ± 0.14^e
ϵ Tau	2.73 ± 0.10	2.63 ± 0.22	2.79 ± 0.11	$2.451^{+0.285}_{-0.034}$	2.40 ± 0.22^f
β Gem	2.08 ± 0.09	1.61 ± 0.54	2.10 ± 0.08	$2.096^{+0.018}_{-0.173}$	1.73 ± 0.17^f
18 Del	2.33 ± 0.05	2.11 ± 0.13	2.35 ± 0.07	$2.257^{+0.039}_{-0.039}$	1.92 ± 0.19^f
γ Cep	1.26 ± 0.14	1.30 ± 0.19	1.19 ± 0.09	$1.379^{+0.054}_{-0.077}$	1.32 ± 0.19^f
HD 5608	1.66 ± 0.08	1.41 ± 0.19	1.72 ± 0.07	1.574 ± 0.040	1.32 ± 0.13^f
κ CrB	1.58 ± 0.08	1.32 ± 0.17	1.53 ± 0.07	$1.551^{+0.032}_{-0.036}$	1.40 ± 0.12^f
6 Lyn	–	–	–	$1.428^{+0.036}_{-0.027}$	1.37 ± 0.14^f
HD 210702	1.71 ± 0.06	1.63 ± 0.13	1.58 ± 0.07	$1.604^{+0.038}_{-0.034}$	1.47 ± 0.14^f
HD 4313	1.53 ± 0.09	1.35 ± 0.11	1.71 ± 0.13	$1.373^{+0.234}_{-0.076}$	$1.61^{+0.13}_{-0.12}g$
HD 5319	1.28 ± 0.10	1.24 ± 0.14	–	$1.278^{+0.089}_{-0.149}$	$1.25^{+0.11}_{-0.10}g$
HD 106270	1.33 ± 0.05	1.33 ± 0.06	–	$1.377^{+0.038}_{-0.037}$	$1.52^{+0.04}_{-0.05}g$
HD 145428	–	–	–	$0.930^{+0.076}_{-0.022}$	$0.99^{+0.10}_{-0.07}$

Table B1 – continued

Star name (1)	Spectroscopy-based grid-based modelling			Asteroseismology	
	Mortier et al. (2013) TS13-SO08 (M_{\odot}) (2) ^a	Mortier et al. (2013) HM07 (M_{\odot}) (3) ^b	Jofré et al. (2015) DS11 (M_{\odot}) (4) ^c	Stock et al. (2018) (M_{\odot}) (5) ^d	(M_{\odot}) (6)
HD 181342	1.70 ± 0.09	1.49 ± 0.19	1.78 ± 0.11	1.380 ± 0.120	$1.73^{+0.18}_{-0.13}$ ^g
HD 185351	–	–	1.82 ± 0.05	$1.687^{+0.043}_{-0.221}$	$1.77^{+0.08}_{-0.08}$ ^g
HD 212771	1.51 ± 0.08	1.22 ± 0.08	1.60 ± 0.13	$1.601^{+0.127}_{-0.247}$	$1.46^{+0.09}_{-0.09}$ ^g

^aLine list by Tsantaki et al. (2013, TS13) are used for stars cooler than 5200 K, while Sousa et al. (2008, SO08) line list is used for hotter stars.

^bLine lists by Hekker & Meléndez (2007, HM07) are used.

^cIron line lists by da Silva et al. (2011, DS11) are used.

^dStock et al. (2018) did not use a line list directly. Instead, they used the T_{eff} , [Fe/H], and $\log g$ values by Hekker & Meléndez (2007).

^eThis work (also listed in Table 2).

^fUpdated values of seismic masses from Stello et al. (2017) (also listed in Table 3). See Section 3.1 for details.

^gNorth et al. (2017).

This paper has been typeset from a $\text{\TeX}/\text{\LaTeX}$ file prepared by the author.